inorganics

MDPI

Article

Combined Effect of Halogenation and SiO_2 Addition on the Li-Ion Conductivity of $LiBH_4$

Valerio Gulino [1,2,*], Laura de Kort [2], Peter Ngene [2], Petra de Jongh [2] and Marcello Baricco [1,*]

[1] Department of Chemistry, NIS-INSTM, University of Turin, Via Pietro Giuria 7, 10125 Torino, Italy
[2] Materials Chemistry and Catalysis, Debye Institute for Nanomaterials Science, Utrecht University, Universiteitsweg 99, 3584 CG Utrecht, The Netherlands; l.m.dekort@uu.nl (L.d.K.); p.ngene@uu.nl (P.N.); p.p.e.dejongh@uu.nl (P.d.J.)
* Correspondence: v.gulino@uu.nl (V.G.); marcello.baricco@unito.it (M.B.)

Abstract: In this work, the combined effects of anion substitution (with Br^- and I^-) and SiO_2 addition on the Li-ion conductivity in $LiBH_4$ have been investigated. Hexagonal solid solutions with different compositions, *h*-$Li(BH_4)_{1-\alpha}(X)_\alpha$ (X = Br, I), were prepared by ball milling and fully characterized. The most conductive composition for each system was then mixed with different amounts of SiO_2 nanoparticles. If the amount of added complex hydride fully fills the original pore volume of the added silica, in both $LiBH_4$-LiBr/SiO_2 and $LiBH_4$-LiI/SiO_2 systems, the Li-ion conductivity was further increased compared to the *h*-$Li(BH_4)_{1-\alpha}(X)_\alpha$ solid solutions alone. The use of $LiBH_4$-LiX instead of $LiBH_4$ in composites with SiO_2 enabled the development of an optimal conductive pathway for the Li ions, since the *h*-$Li(BH_4)_{1-\alpha}(X)_\alpha$ possesses a higher conductivity than $LiBH_4$. In fact, the Li conductivity of the silica containing *h*-$Li(BH_4)_{1-\alpha}(X)_\alpha$ is higher than the maximum reached in $LiBH_4$-SiO_2 alone. Therefore, a synergetic effect of combining halogenation and interface engineering is demonstrated in this work.

Keywords: complex hydrides; solid-state electrolytes; $LiBH_4$

check for updates

Citation: Gulino, V.; de Kort, L.; Ngene, P.; de Jongh, P.; Baricco, M. Combined Effect of Halogenation and SiO_2 Addition on the Li-Ion Conductivity of $LiBH_4$. *Inorganics* **2023**, *11*, 459. https://doi.org/10.3390/inorganics11120459

Academic Editor: Christian Julien

Received: 7 October 2023
Revised: 18 November 2023
Accepted: 24 November 2023
Published: 26 November 2023

1. Introduction

Today, much effort is devoted to increasing the safety of Li-ion batteries, making electrolytes more stable in temperature and less prone to decomposition, limiting in such a way the flammability risk [1]. Solid-state electrolytes were proposed as candidates that are intrinsically able to overcome such limitations. Their thermal conductivity, generally higher for a solid than for a liquid, might avoid the formation of hot spots when high currents are required, and consequently limiting thermal runaway [2,3]. The use of solid electrolytes in an all-solid-state Li-ion battery can also allow for the use of Lithium metal as an anode, replacing the conventional graphite anode [4]. In fact, Lithium metal possesses a significantly higher theoretical specific capacity (3862 mA hg^{-1}) with respect to graphite (372 mA hg^{-1}), leading to a substantial gain of both gravimetric and volumetric energy density of batteries [5,6].

Lithium borohydride ($LiBH_4$), a low-density (0.666 g/cm^3) material, has been extensively studied as a solid electrolyte, since the discovery of its remarkable ionic conductivity (σ) above 120 °C [7]. The room temperature (*RT*) polymorph of $LiBH_4$ has an orthorhombic unit cell (*o*-$LiBH_4$); space group (s.g.), *Pnma*; and low ionic conductivity (around 10^{-8} S cm^{-1}), while, after a phase transition at 110 °C, the high-temperature polymorph (*h*-$LiBH_4$) has a hexagonal unit cell (s.g. $P6_3mc$) [8] and shows high ionic conductivity (~10^{-3} S cm^{-1} at 120 °C) [9]. The activation energy (E_A) for Li-ion conductivity reported in the literature for the orthorhombic $LiBH_4$ is 0.75 ± 0.07 eV [10]. Recently, the electrochemical stability of $LiBH_4$ has been reported to be up to about 2.0 V vs. Li^+/Li [11,12].

Different approaches have been adopted to enhance the *RT* Li-ion conductivity in $LiBH_4$ [7]. Halide substitution, replacing BH_4^- with I^-, Br^- and Cl^-, stabilizes the hexago-

nal $LiBH_4$ by forming solid solutions (SSs) [11,13–15]. Mixing $LiBH_4$ with other complex anions (e.g., NH_2^- and NH^{2-}) leads to the formation of compounds with different structures, and improved ionic conductivity at R*T* [16,17]. Making borohydride–oxide composites, by nanoconfinement of $LiBH_4$ in suitable scaffolds, also leads to highly improved R*T* Li-ion conductivity [18–21]. The enhanced Li-ion conductivity relies on the formation of a conductive interface, which can be described with a core–shell model [22,23]. The fraction of $LiBH_4$ (the core) in direct contact with the oxide (the shell) forms an interfacial layer, featuring an increased Li-ion conductivity. In the $LiBH_4$-SiO_2 system, Li conductivity is optimized when $LiBH_4$ completely fills the oxide pores [21], and the thickness of the conductive interfacial layer has been estimated to be around 1–2 nm [24]. In addition, different $LiBH_4$-oxide composite systems ($LiBH_4$-ZrO_2, $LiBH_4$-MgO and $LiBH_4$-$LiBF_4$) have been prepared by ball milling, showing improved R*T* conductivity (~10^{-4} S cm^{-1}) with respect to the *o*-$LiBH_4$, thanks to a suitable interface engineering [19–21].

Recently, it has been reported that halogenation and nanoconfinement can be combined to further enhance the ionic conductivity of $LiBH_4$ [25,26]. However, the exact interplay between the composition of the hexagonal SS and the confinement in the oxide was not fully unraveled. In fact, only a single composition of *h*-$Li(BH_4)_{1-\alpha}(I)_\alpha$ SSs in combination with silica was studied in Ref. [26]. The aim of this work is to extend the study to the effect of the SiO_2 content in both $LiBH_4$-LiI/SiO_2 and $LiBH_4$-LiBr/SiO_2 nanocomposites. The goal is to obtain a deeper understanding of the synergetic effects arising between halogenation and interface engineering on the ionic conductivity of ion-substituted metal hydride/oxide nanocomposites, which are quite promising electrolytes for all-solid-state batteries. The results show that the amount of SiO_2, LiI, LiBr and $LiBH_4$ has a significant influence on the ionic conductivity, and optimizing the composition is thus crucial for obtaining high-conductivity nanocomposites, making them suitable for all-solid-state batteries.

2. Experimental Section

2.1. Synthesis

$LiBH_4$ (purity > 95%, from Sigma-Aldrich, St. Louis, MO, USA), LiBr (purity > 99%, from Sigma-Aldrich) and LiI (purity > 99%, from Sigma-Aldrich) were mechanochemically treated in different ratios, to stabilize the hexagonal SSs at R*T*. Before mixing, LiBr was dried at 120 °C in a furnace under a dynamic vacuum, while LiI was already purchased in an inert atmosphere. A Fritsch Pulverisette 6 planetary mill was used to ball mill the reactants under an argon atmosphere in 80 mL tungsten carbide vials, with tungsten carbide balls (10 mm diameter) and a ball-to-sample mass ratio of 30:1. All $LiBH_4$-LiX (X = Br, I) mixtures were ball milled for 1.5 h at 350 r.p.m., in steps of 10 min, separated by 2 min breaks, to minimize possible heating effects [11]. Samples were annealed at 250 °C for 2 or 4 h in a quartz tube under a static vacuum, with a heating/cooling rate of 5 °C/min, to reach the equilibrium conditions. Thereafter, samples were mixed with SiO_2 (Aerosil 300, Evonik, Essen, Germany) by ball milling. Prior to mixing, SiO_2 was pelletized and dried at 300 °C for 6 h under a dynamic vacuum, to remove any physisorbed/chemisorbed water. All *h*-$Li(BH_4)_{1-\alpha}(X)_\alpha$-$SiO_2$ composites were ball milled at 300 r.p.m. for three 10 min intervals, separated by 1 min breaks. All manipulations were performed in an argon-filled glovebox (MBraun Lab Star Glove Box supplied with pure 5.5 grade argon, <1 ppm O_2, <1 ppm H_2O). The nomenclature and compositions of prepared samples are reported in Table 1.

The density of SiO_2 has been taken as 2.20 g/cm^3 from the literature [27]. The surface properties and porosity of the SiO_2 were obtained by N_2 adsorption at 77 K in a TriStar Plus II gas-volumetric apparatus (Micromeritics, Norcross, GA, USA). The specific surface area (S_{BET}) was calculated by fitting with a Brunauer–Emmett–Teller isotherm [28], and it turned out to be equal to 294 m^2/g. The total pore volume (V_p) was derived from the absorbed volume of the nitrogen at p/p_0 = 0.95 and it was determined to be 2.30 cm^3/g.

Table 1. Composition, fraction of pore filling and thickness of $LiBH_4$ of investigated samples.

Name	Halide		Oxide		ρ [1]	Fraction of Pore Filling [2]	Thickness of h-Li$(BH_4)_{1-\alpha}(X)_\alpha$ [3]
	Molar Fraction		wt.%	*v*/*v* %	g/cm^3	%	nm
I0.2	I	0.2	/	/	1.30	/	/
I0.2-13	I	0.2	20	13	1.30	134	10.5
I0.2-16	I	0.2	25	16	1.30	100	7.8
I0.2-20	I	0.2	30	20	1.30	78	6.1
I0.2-33	I	0.2	45	33	1.30	41	3.2
I0.2-47	I	0.2	60	47	1.30	22	1.7
I0.3	I	0.3	/	/	1.66	/	/
I0.3-24	I	0.3	30	24	1.66	61	4.8
I0.3-38	I	0.3	45	38	1.66	32	2.5
I0.4	I	0.4	/	/	1.95	/	/
I0.4-28	I	0.4	30	28	1.95	52	4.1
I0.4-42	I	0.4	45	42	1.95	27	2.1
I0.5	I	0.5	/	/	2.23	/	/
I0.5-45	I	0.5	45	45	2.23	24	1.9
Br0.3	Br	0.3	/	/	1.36	/	/
Br0.3-13	Br	0.3	20	13	1.36	128	10.0
Br0.3-21	Br	0.3	30	21	1.36	75	5.8
Br0.3-34	Br	0.3	45	34	1.36	39	3.1
Br0.3-48	Br	0.3	60	48	1.36	21	1.7
Br0.4	Br	0.4	/	/	1.60	/	/
Br0.4-24	Br	0.4	30	24	1.60	63	5.0
Br0.4-37	Br	0.4	45	37	1.60	33	2.6
Br0.5	Br	0.5	/	/	1.83	/	/
Br0.5-26	Br	0.5	30	26	1.83	55	4.3
Br0.5-40	Br	0.5	45	40	1.83	29	2.3

[1] Calculation performed using the h-Li$(BH_4)_{1-\alpha}(X)_\alpha$ volume obtained from the Rietveld refinement. [2] Calculation was performed dividing the h-Li$(BH_4)_{1-\alpha}(X)_\alpha$ occupied volume per gram of SiO_2 by the pore volume (V_p). [3] Calculation was performed considering the BET surface area of the SiO_2 and assuming it as a plane.

2.2. Powder X-ray Diffraction (PXD)

Powdered samples were characterized by PXD at R*T* using a Panalytical X-pert Pro MPD (Cu $K_{\alpha1}$ = 1.54059 Å, $K_{\alpha2}$ = 1.54446 Å) in Debye–Scherer geometry. Patterns were collected from the 10° to 70° 2θ range, with a step size of 0.016. Glass capillaries (0.5 mm) were filled with the sample powder and sealed under an Ar atmosphere. The Rietveld refinement of diffraction patterns was performed using Materials Analysis Using Diffraction (MAUD) software v 2.992 [29], considering R_{wp} and χ as indicators for the quality of the fitting.

2.3. Electrochemical Impedance Spectroscopy (EIS)

The total conductivity was measured with electrochemical impedance spectroscopy (EIS) using a PARSTAT 2273 potentiostat (frequency range of 1 Hz–1 MHz, applied voltage of 10 mV rms), with the measuring cell placed inside an Ar-filled glovebox. Using an axial hydraulic press, samples were compacted into pellets (diameter of 13 mm, thickness of 1−2 mm) with about 200 MPa pressure. Lithium foils (Sigma-Aldrich, purity of 99.9%, 0.38 mm thick) were used as non-blocking electrodes. EIS was performed every 10 °C in the temperature range of R*T* < T < 130 °C during the heating ramp and every 20 °C during cooling. The impedance spectra showed a single arc in the Nyquist plot; therefore, they were all fitted using an (RQ) equivalent circuit model, i.e., a resistance in parallel with a constant phase element (CPE). Impedance data were analyzed via EqC software v. 0.6 rev.2 [30], following the data validation described in Ref. [31]. All fits performed resulted in a chi-squared test (χ^2 test) < 10^{-3}. Because the electronic conduction is very low, the measured conductivity was assigned entirely to Li-ion conductivity, as demonstrated previously [21,32].

3. Results and Discussion

3.1. h-Li(BH$_4$)$_{1-x}$X$_x$ Solid Solutions

The reported values of the solubility limits for h-Li(BH$_4$)$_{1-\alpha}$(Br)$_\alpha$ SSs are $0.30 \leq \alpha \leq 0.5$ [11,33], and for h-Li(BH$_4$)$_{1-\alpha}$(I)$_\alpha$ SSs, they are $0.18 \leq \alpha \leq 0.50$ [13]. A range of h-Li(BH$_4$)$_{1-\alpha}$(Br)$_\alpha$ samples, containing 0.30, 0.40 and 0.50 molar fractions of LiBr (denoted as **Br0.3**, **Br0.4** and **Br0.5**), and of h-Li(BH$_4$)$_{1-\alpha}$(I)$_\alpha$ samples, containing 0.20, 0.30, 0.40 and 0.50 molar fractions of LiI (denoted as **I0.2**, **I0.3**, **I0.4** and **I0.5**), were synthetized. Diffraction patterns collected after the synthesis are shown in Figure 1a,b. A single crystalline phase was found for all synthetized samples, namely h-Li(BH$_4$)$_{1-\alpha}$(Br)$_\alpha$ (Figure 1a) and h-Li(BH$_4$)$_{1-\alpha}$(I)$_\alpha$ (Figure 1b). Neither cubic halides (c-LiBr or c-LiI) nor o-LiBH$_4$ starting materials were detected. These results were expected, as the chosen compositions are in the solubility range of hexagonal SSs reported in the literature [11,33].

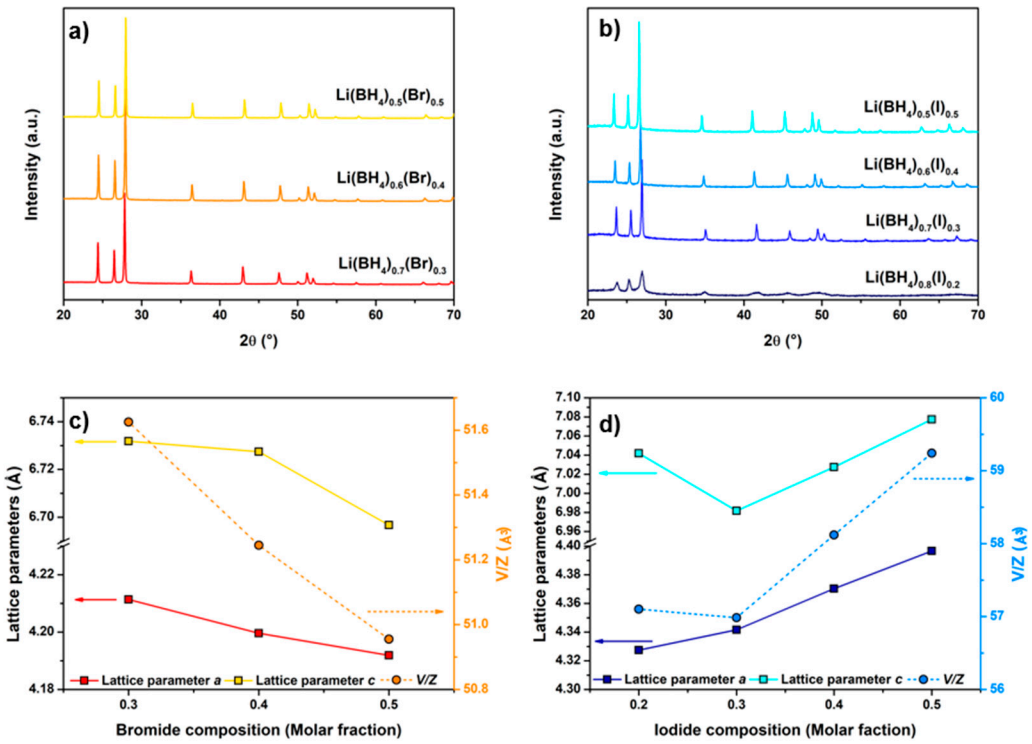

Figure 1. PXD patterns of (**a**) **Br0.3**, **Br0.4** and **Br0.5** samples and (**b**) **I0.2**, **I0.3**, **I0.4** and **I0.5** samples. Lattice parameters (**a**,**c**) and unit cell volume (V/Z) of the hexagonal (P63mc) structure as a function of the halide content (molar fraction) of (**c**) h-Li(BH$_4$)$_{1-\alpha}$(Br)$_\alpha$ and (**d**) h-Li(BH$_4$)$_{1-\alpha}$(I)$_\alpha$.

Using Rietveld refinement, all patterns were analyzed in detail. A structural model for the hexagonal polymorph of LiBH$_4$ (P63mc) was used to describe the structure of h-Li(BH$_4$)$_{1-\alpha}$(X)$_\alpha$ SSs, where Br^- or I^- ions were considered to be located in correspondence with the boron position (i.e., 2b Wyckoff site). The obtained lattice parameters (a and c) and unit cell volume (V/Z) of the hexagonal phase, obtained from the Rietveld refinement of the PXD patterns, are reported in Figure 1c,d, as a function of the halide content, for the LiBH$_4$-LiBr and LiBH$_4$-LiI systems, respectively. Figure 1c shows that both the lattice parameters, as well as the unit cell volume, decrease with increasing bromide concentration. The opposite behavior is observed for the LiBH$_4$-LiI system, as highlighted in Figure 1d, which demonstrates how the lattice parameters and the unit cell volume expand when the iodide concentration increases above 0.3.

The value of cell volume for the hexagonal pure LiBH$_4$ was estimated at RT by using the volumetric thermal expansion coefficient (2.9×10^{-4} K^{-1}) [34], and it turned out to be equal to 106.5 Å^3, corresponding to a unit cell volume (V/Z) of 53.3 Å^3. The extrapolated RT cell volume of pure h-LiBH$_4$ is larger than that of sample **Br0.3** (51.6 Å^3) and even

larger than **Br0.4** and **Br0.5**. In fact, a contraction of the cell volume of the hexagonal SS is expected after halogenation, considering the smaller ionic radius of Br^- compared to BH_4^- (Br^- = 1.96 Å, BH_4^- = 2.03 Å) [35]. On the contrary, considering the h-$Li(BH_4)_{1-\alpha}(I)_\alpha$ SSs, the volume of sample **I0.2** (57.0 $Å^3$) is larger than the RT extrapolated volume of h-$LiBH_4$, indicating an expansion of the lattice. The expansion of the hexagonal lattice is even more pronounced for increased I^- content, as observed for samples **I0.3**, **I0.4** and **I0.5**. In this case, the expansion is due to the larger anion radius of I^- compared to BH_4^- (I^- = 2.20 Å, BH_4^- = 2.03 Å) [35].

As expected, both lattice constants and unit cell volume decrease monotonically as a function of composition for the $LiBH_4$-LiBr system, as shown in Figure 1c. On the contrary, Figure 1d shows that lattice parameter a linearly increases with the iodide concentration, while lattice parameter c is found to shrink when increasing the iodide content up to 0.3 and then to expand between 0.3 and 0.5. This nonmonotonic evolution of the c-axis seems illogical, but it was already reported by Sveinbjörnsson et al. [13], and it has been explained by the possible formation of some intermediate phases [13,36]. This could also be the origin of the asymmetric peak shape and peak broadening observed in Figure 1b for sample **I0.2**. A more detailed crystal structure analysis on this sample would be necessary to define the exact structure and explain this nonmonotonic expansion of the c-axis. Considering the I^- concentration above 0.3, the expansion of the c-axis is as expected, in agreement with the values previously reported [37,38].

The effect of halogenation on the vibrational properties was explored with IR-ATR spectroscopy (see Supporting Information for experimental details) and the results are shown in Figure S1a for h-$Li(BH_4)_{1-\alpha}(Br)_\alpha$ SSs and in Figure S1b for h-$Li(BH_4)_{1-\alpha}(I)_\alpha$ SSs, together with the spectrum for pure orthorhombic $LiBH_4$. The stabilization of the high-temperature hexagonal polymorph of $LiBH_4$, through anion substitution, results in a general broadening of both B-H stretching and bending bands. Increasing the halide content, the B-H stretching bands progressively merge in a single and broad band, reflecting an increase in the lattice distortion and disordering effects, as discussed in Refs. [37,39].

To investigate the trend of Li-ion conductivity as a function of the SSs' composition, temperature-dependent EIS measurements were performed in the temperature range of 30 < T < 130 °C and an example of EIS spectra can be seen in Figure S2. Figure 2 shows the Li^+ conductivities, as a function of the inverse temperature, for all samples, including pure $LiBH_4$ for comparison.

As expected, for hexagonal SSs, the change in the conductivity due to the polymorphic transition above 110 °C, as observed for pure $LiBH_4$, disappears. In the h-$Li(BH_4)_{1-\alpha}(Br)_\alpha$ system (Figure 2a), sample **Br0.3**, i.e., h-$Li(BH_4)_{0.7}(Br)_{0.3}$, shows the highest value for conductivity at 30 °C (1.8×10^{-6} S cm^{-1}), while in the h-$Li(BH_4)_{1-\alpha}(I)_\alpha$ system (Figure 2b) is the sample **I0.2**, i.e., h-$Li(BH4)_{0.8}(I)_{0.2}$, that shows the highest Li-ion conductivity (3.6×10^{-5} S cm^{-1} at 30 °C). It is worth noting that these values are three and four orders of magnitude higher than that of pure $LiBH_4$ at RT, respectively. Before the phase transition, all samples show higher Li-ion conductivity with respect to $LiBH_4$, confirming that halogenation is a robust approach to enhance the Li-ion conductivity of the $LiBH_4$.

A correlation between composition and ionic transport properties exists, and in general, the incorporation of a halide results in an enhanced conductivity compared to $LiBH_4$ [11,15]. However, increasing the halide/BH_4 ratio decreases the Li-ion conductivity. These results indicate that the presence of BH_4^- anions in the structure promotes Li-ion mobility. In fact, the higher Li-ion conductivity of the h-$LiBH_4$, compared to the orthorombic structure, is due to the rapid reorientation of the BH_4^- anions, i.e., a higher frequency of rotational jumps [40,41]. This is in agreement with our results, where increasing the halide concentration causes a decrease in the Li-ion conductivity, both for the incorporation of I- as well as Br-.

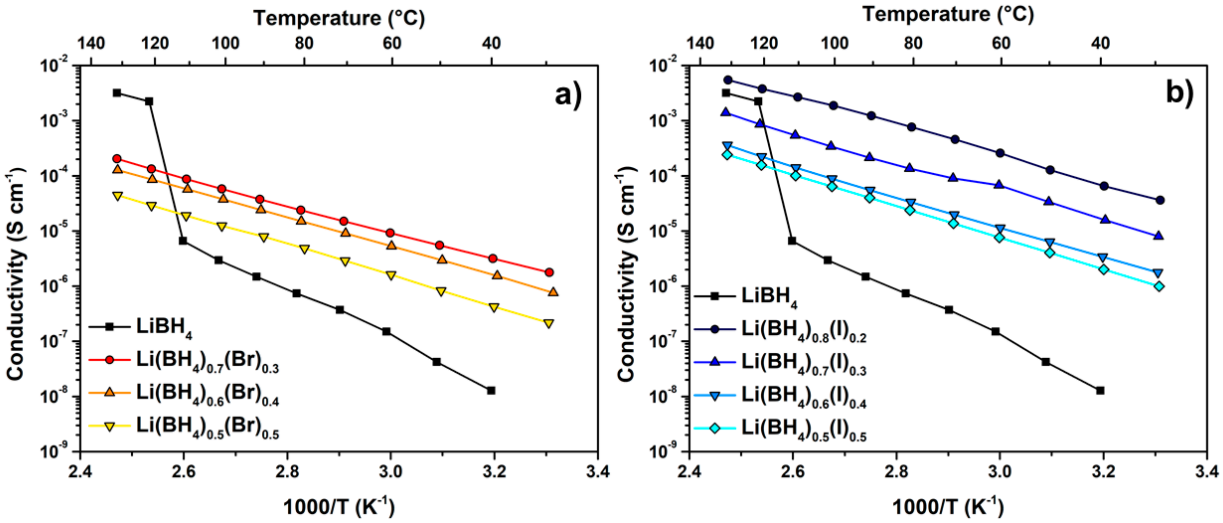

Figure 2. Li-ion conductivity of (**a**) **Br0.3**, **Br0.4** and **Br0.5** samples and (**b**) **I0.2**, **I0.3**, **I0.4 and I0.5** samples. All data were obtained from the second heating temperature-dependent EIS cycle. The Li-ion conductivity of the $LiBH_4$ during the second heating temperature-dependent EIS cycle is shown for comparison. The impedance spectroscopy measurements result in a Nyquist plot showing a single arc.

Activation energies have been calculated based on the data shown in Figure 2, and they are shown in Figure 3, as a function of the h-Li$(BH_4)_{1-\alpha}(X)_\alpha$ halide content. Figure S3 shows an example of the linear fit used to calculate the activation energies. The lowest activation energy was observed for both h-Li$(BH_4)_{1-\alpha}(X)_\alpha$ SSs when α = 0.3 (i.e., 0.517 ± 0.01 eV for sample **Br0.3** and 0.54 ± 0.03 eV for sample **I0.3**). Above α = 0.3, the activation energy increases. Unexpected behavior is evidenced for sample **I0.2**, i.e., h-Li$(BH_4)_{0.8}(I)_{0.2}$, which shows the highest conductivity, but it has an activation energy higher than that of sample **I0.3**. This behavior could be linked to the nonmonotonic expansion of the c-axis and/or to the not completely ordered structure of the h-Li$(BH_4)_{0.8}(I)_{0.2}$ SS (Figure 1d) [13].

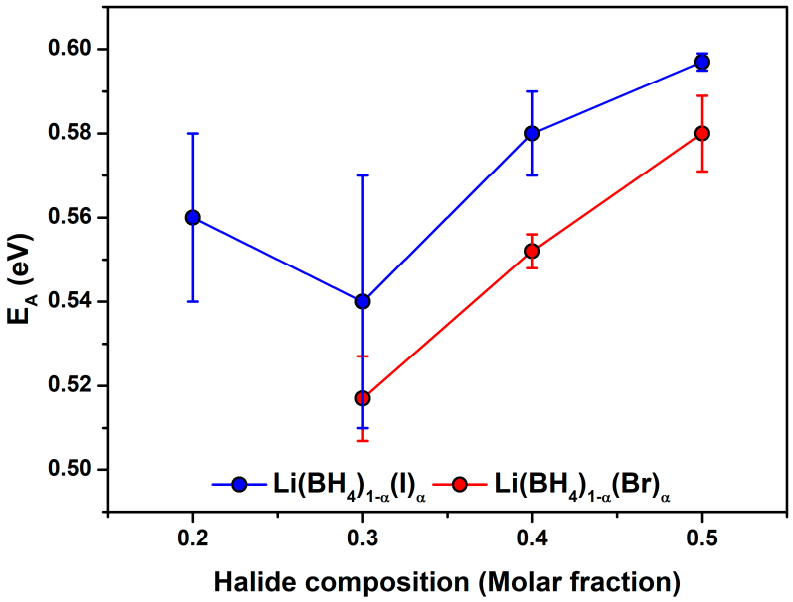

Figure 3. Activation energy as a function of halide concentration in the h-Li$(BH_4)_{1-\alpha}(X)_\alpha$ (X = Br, I) SSs. The activation energy was calculated from data collected during the second heating ramp. Error bars were obtained from the linear fit of the Arrhenius plot (95% confidence).

As a conclusion, the incorporation of halide ions in the $LiBH_4$ structure leads to the stabilization of the hexagonal phase, thereby improving Li-ion conductivity. The extent of this improvement depends on the exact solid solution composition, becoming smaller with increasing halide content.

3.2. *(h-Li$(BH_4)_{1-\alpha}(X)_\alpha)_{1-\beta}$-$(SiO_2)_\beta$ Systems*

Table 1 (see experimental section) shows v/v % of SiO_2 and the corresponding pore filling fraction of the (h-Li$(BH_4)_{1-\alpha}(X)_\alpha)_{1-\beta}$-$(SiO_2)_\beta$ synthesized samples. The values of β (i.e., v/v % of SiO_2) have been calculated considering densities of h-Li$(BH_4)_{1-\alpha}(X)_\alpha$ SSs, as calculated from the cell volume data obtained with Rietveld refinement of PXD patterns (Figure S4). The SiO_2 pore filling fraction was calculated as the ratio between the volume of $Li(BH_4)_{1-\alpha}(X)_\alpha$ SSs and the total pore volume of the SiO_2.

h-$Li(BH_4)_{0.7}(Br)_{0.3}$ and h-$Li(BH_4)_{0.8}(I)_{0.2}$ showed the highest Li-ion conductivity; therefore, the effect of SiO_2 content in these composites was analyzed in more detail. After the synthesis, the PXD patterns were collected at RT for each sample (Figure S5; Figure S5a shows the PXD pattern of h-$Li(BH_4)_{0.7}(Br)_{0.3}$ mixed with different v/v % of SiO_2, while Figure S5b shows the PXD pattern of h-$Li(BH_4)_{0.8}(I)_{0.2}$-SiO_2 composites). Considering that SiO_2 is amorphous, from results reported in Figure S5, it is possible to assume the absence of both h-$Li(BH_4)_{1-\alpha}(X)_\alpha$ SSs' structural modifications, due to the mechanochemical treatment, and the formation of new compounds. So, the PXD analysis clearly indicates no interactions between the $Li(BH_4)_{1-\alpha}(X)_\alpha$ SSs and SiO_2.

Additional structural/chemical information was obtained using vibrational (ATR-IR) measurements. From the ATR-IR spectra of the (h-Li$(BH_4)_{1-\alpha}(X)_\alpha)_{1-\beta}$-$(SiO_2)_\beta$ composites shown in Figure S6, the absorption bands related to B-H stretching (2400–2000 cm^{-1} region) of both h-$Li(BH_4)_{1-\alpha}(X)_\alpha$ SSs are not affected significantly by the mechanochemical treatment with SiO_2, showing a rather similar shape with the bands already reported in Figure S1. This result supports the PXD results, which indicate that the addition of SiO_2 did not lead to noticeable changes in the structural properties of the h-$Li(BH_4)_{1-\alpha}(X)_\alpha$.

It is worth noting that an electrochemical stability of 2.5 V has been observed for h-$Li(BH_4)_{0.8}(I)_{0.2}$ mixed with 16 v/v % of SiO_2, which is higher than that of $LiBH_4$ alone (2.2 V) [26]. The effect of silica addition to the h-$Li(BH_4)_{1-\alpha}(X)_\alpha$ SSs on the Li-ion conductivity of all the prepared samples was determined using EIS measurements. The Li-ion conductivity as a function of the inverse temperature in h-$Li(BH_4)_{0.7}(Br)_{0.3}$ and h-$Li(BH_4)_{0.8}(I)_{0.2}$ SSs, with different v/v % of SiO_2, is shown in Figure 4.

Results show that the Li-ion conductivity is enhanced upon SiO_2 addition, when the SiO_2 content is lower than 21 v/v % for h-$Li(BH_4)_{0.7}(Br)_{0.3}$ and 20% for h-$Li(BH_4)_{0.8}(I)_{0.2}$, respectively. These volume fractions correspond to the filling of more than 75% and 78% of the original SiO_2 total pore volume (2.30 cm^3/g) in the case of h-$Li(BH_4)_{0.7}(Br)_{0.3}$ and h-$Li(BH_4)_{0.8}(I)_{0.2}$, respectively. Among all h-$Li(BH_4)_{0.8}(I)_{0.2}$-SiO_2 mixtures (Figure 4b), those with v/v % of SiO_2 between 13% and 20% show very similar conductivities ($9.3 \times 10^{-5} \div 1.1 \times 10^{-4}$ S cm^{-1} at 40 °C), indicating that the addition of a small amount of silica has a small effect on the Li-ion conductivity. Similar behavior was observed for h-$Li(BH_4)_{0.7}(Br)_{0.3}$-SiO_2 mixtures (Figure 4a), even though the composite containing 13 v/v % of SiO_2 shows a more evident enhancement of the Li-ion conductivity with respect to the h-$Li(BH_4)_{0.7}(Br)_{0.3}$ SS, reaching a Li-ion conductivity of 4.9×10^{-5} S cm^{-1} at 40 °C. On the other hand, for composites containing v/v % of SiO_2 higher than 21, the Li-ion conductivity decreases with respect to the SS alone for both h-$Li(BH_4)_{0.7}(Br)_{0.3}$ and h-$Li(BH_4)_{0.8}(I)_{0.2}$ composites.

To better understand the trend in the Li-ion conductivity as a function of SiO_2 content (shown in Figure 4), the dependence of the Li conductivity at 40 °C, as well as that of the E_A, is shown in Figure 5 as a function of the SiO_2 pore filling fraction.

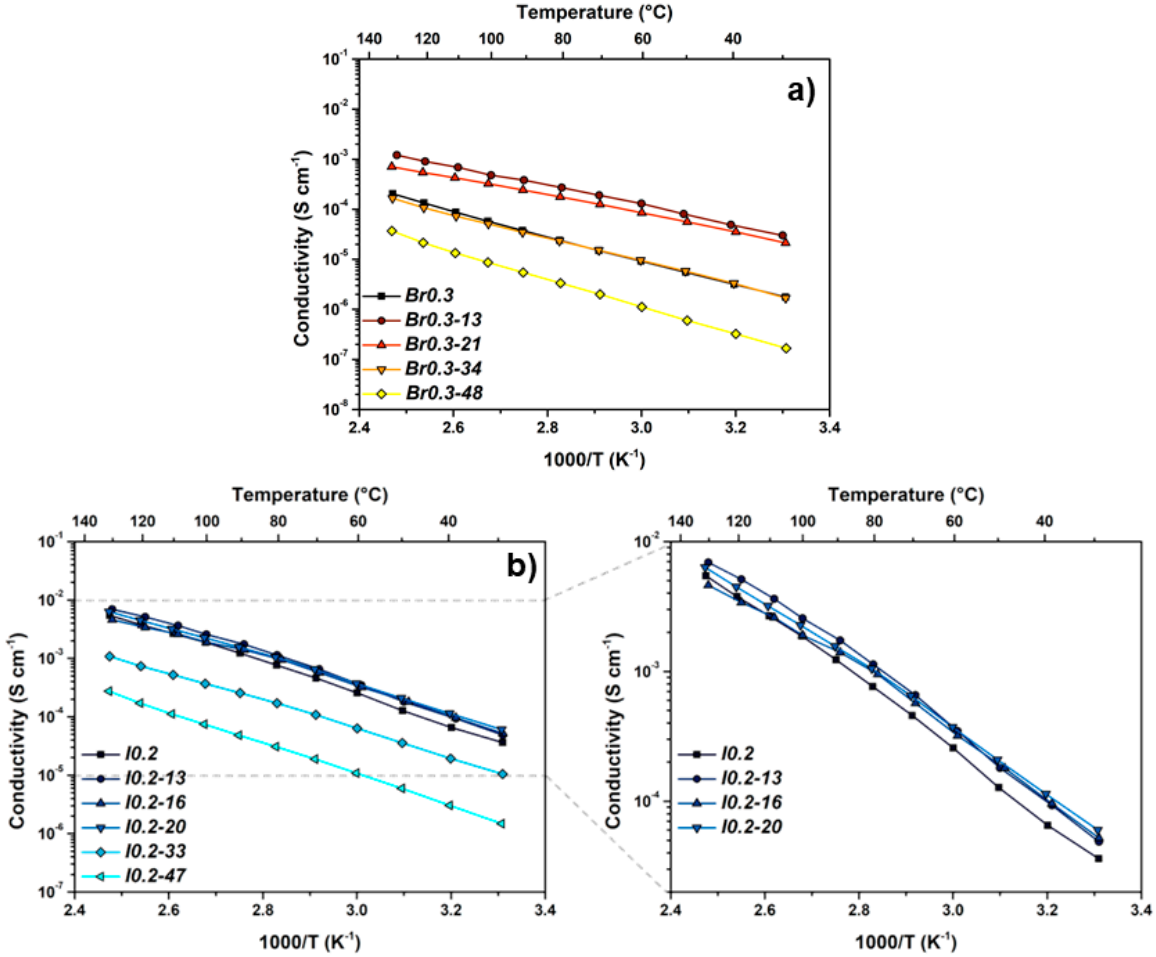

Figure 4. Li-ion conductivities of (**a**) h-Li$(BH_4)_{0.7}(Br)_{0.3}$ and (**b**) h-Li$(BH_4)_{0.8}(I)_{0.2}$ samples, with different v/v % of SiO_2. Data were obtained from the second heating temperature-dependent EIS cycle. An enlargement of the vertical axes of figure (**b**) is also shown. The Li-ion conductivities of (**a**) h-Li$(BH_4)_{0.7}(Br)_{0.3}$ and (**b**) h-Li$(BH_4)_{0.8}(I)_{0.2}$ samples during the second heating temperature-dependent EIS cycle are reported for comparison.

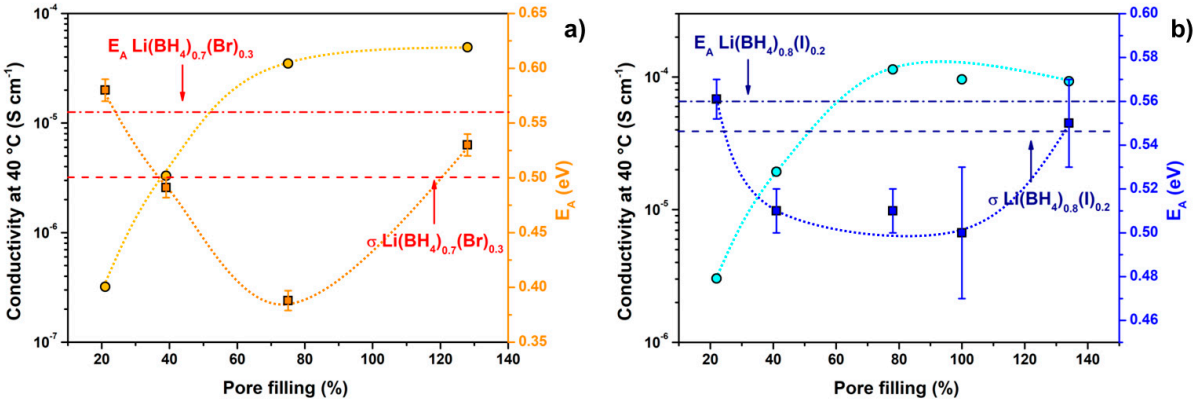

Figure 5. Li-ion conductivity at 40 °C (circles) and activation energy (squares) as a function of pore filling fraction (%) for (**a**) h-Li$(BH_4)_{0.7}(Br)_{0.3}$ and (**b**) h-Li$(BH_4)_{0.8}(I)_{0.2}$ SSs, with different v/v % of SiO_2. Dashed lines indicate the Li-ion conductivity at 40 °C of the h-Li$(BH_4)_{1-\alpha}(X)_\alpha$ hexagonal phases without oxide; dash–dotted lines correspond to the activation energy calculated for the h-Li$(BH_4)_{1-\alpha}(X)_\alpha$ SSs without oxide; dotted lines are a guide for the eye.

Figure 5 shows that the Li-ion conductivity increases with the pore filling, reaching a nearly constant value when it is higher than 80%. For a pore filling >20%, the E_A is lower than that obtained for the hexagonal SSs without SiO_2 and the lowest value of activation energy is observed for the sample containing an amount of h-Li$(BH_4)_{1-\alpha}(X)_\alpha$ close to 100% of the pore volume of the SiO_2. Finally, a complete overview of the conductivity of the composites synthesized is provided in Figure 6, which highlights how the combination of halide concentration and SiO_2 content affects the Li-ion conductivity.

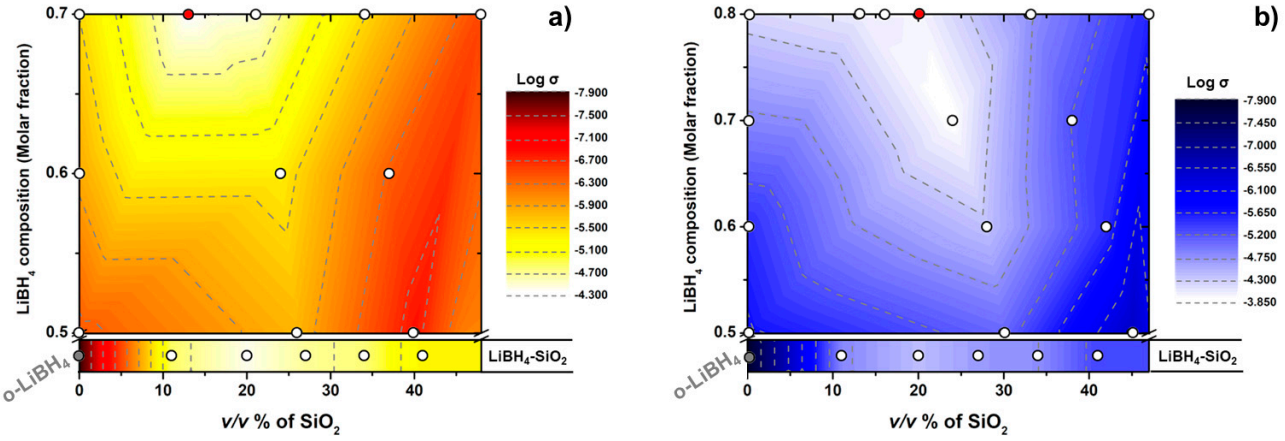

Figure 6. Contour map of Log σ at 40 °C as a function of the amount of SiO_2 and of (**a**) h-Li$(BH_4)_{1-\alpha}(Br)_\alpha$ and (**b**) h-Li$(BH_4)_{1-\alpha}(I)_\alpha$ composition. Iso-conductivity dashed lines correspond to the values and lines shown in the legend. The red circles indicate the highest Log σ reached in each system. In the bottom of both figures, the grey circle indicates the Log σ of the o-$LiBH_4$, while white circles give the Log σ values of $LiBH_4$-SiO_2 composites, as taken from Ref. [21].

For both systems, a synergetic effect occurs when the fraction of SiO_2 is between 20 and 30 v/v %, and the maximum Li-ion conductivity is reached for samples with SSs with the highest BH_4^- content. The maximum (highlighted with the red point in Figure 6) of the Li conductivity reached in both (h-Li$(BH_4)_{1-\alpha}(X)_\alpha)_{1-\beta}$-$(SiO_2)_\beta$ systems is higher than the maximum reached in the $LiBH_4$-SiO_2 (taken from Ref. [21]).

3.3. Synergetic Effect

The enhancement of the Li-ion conductivity of $LiBH_4$ with the addition of SiO_2 can be explained with a core–shell model, different from what was reported for a polymer electrolyte [42], where two different conductive phase fractions are present: the first is at the interface, in direct contact with the oxide, and highly conductive, and the second fraction is in the bulk, maintaining the low conductivity of the orthorhombic phase [21,23,43]. This core–shell model can also be applied to both (h-Li$(BH_4)_{1-\alpha}(X)_\alpha)_{1-\beta}$-$(SiO_2)_\beta$ systems considered here, since the conductivities of the h-Li$(BH_4)_{1-\alpha}(X)_\alpha$ can be enhanced by a certain amount of SiO_2. More specifically, in samples for which too much SiO_2 is added (with the hydride present corresponding to a silica pore filling below 70%), the insulator (i.e., SiO_2) interrupts the Li-ion pathway of the highly conductive interface layer, leading to a conductivity that is lower than the h-Li$(BH_4)_{1-\alpha}(X)_\alpha$ SS without silica. The E_A obtained for these samples (i.e., containing an excess of silica) is similar to that of the pure h-Li$(BH_4)_{1-\alpha}(X)_\alpha$, indicating that the Li-ion conductivity is dominated by the conduction inside the h-Li$(BH_4)_{1-\alpha}(X)_\alpha$ SSs.

Interestingly, a high Li-ion conductivity is observed even when the volume of the h-Li$(BH_4)_{1-\alpha}(X)_\alpha$ exceeds the SiO_2 pore volume (pore filling > 100%). Differently from the $LiBH_4$-SiO_2 system (see Figure 6), when the volume of h-Li$(BH_4)_{1-\alpha}(X)_\alpha$ SS exceeds the pore volume (pore filling > 100%), the interface layer is interrupted no more by the low-conductive o-$LiBH_4$, but the connectivity of the Li-ion pathway is provided by the high-conductive h-Li$(BH_4)_{1-\alpha}(X)_\alpha$ SS [23]. In addition, the calculated values of the E_A

show that, when the amount of hydride exceeds the complete pore filling, it returns to be comparable to that of h-Li$(BH_4)_{1-\alpha}(X)_\alpha$ SSs without silica, indicating that the excess of the SS dominates the conduction mechanism. Therefore, since the h-Li$(BH_4)_{1-\alpha}(X)_\alpha$ SSs display a rather good conductivity, an excess of it does not negatively impact the conductivity of the composites.

This work underlines that the combination of different approaches to increase the Li-ion conductivity is a powerful method to obtain novel solid-state electrolytes to be used in all-solid-state batteries. At the same time, a clear trend between the amount of SiO_2 and Li-ion conductivity was determined.

4. Conclusions

In this work, the effect of halide composition on the Li-ion conductivity of h-Li$(BH_4)_{1-\alpha}(X)_\alpha$ has been investigated for the $LiBH_4$-LiI and $LiBH_4$-LiBr systems. Once the most conductive composition for each system was determined, the effect of adding SiO_2 was investigated. In the $LiBH_4$-LiX/SiO_2 systems, the Li-ion conductivity was further increased if the amount of hydride added corresponded to the original pore volume of the silica in the composite. The use of $LiBH_4$-LiX instead of $LiBH_4$ in the SiO_2-containing composites ensured an optimal pathway for fast Li-ion conduction due to the higher conductivity of $LiBH_4$-LiX SSs compared to $LiBH_4$. The Li-conductivity of the halide-containing composites was higher than that of $LiBH_4$-SiO_2 [21] (at 40 °C, 1.1×10^{-4} S cm^{-1} for h-Li$(BH_4)_{0.8}(I)_{0.2}$—13 v/v % of SiO_2 vs. 4.1×10^{-5} S cm^{-1} for $LiBH_4$—20 v/v % of SiO_2). Thus, a synergetic effect of combining halogenation and interface engineering is demonstrated in this work.

Supplementary Materials: The following supporting information can be downloaded at: https://www.mdpi.com/article/10.3390/inorganics11120459/s1, Figure S1: IR−ATR spectrum of *h*-Li$(BH_4)_{1-\alpha}(X)_\alpha$ SSs and pure $LiBH_4$; Figure S2: Density of h-Li$(BH_4)_{1-\alpha}(X)_\alpha$ SSs as a function of halide concentration; Figure S3: PXD patterns of *h*-Li$(BH_4)_{1-\alpha}(X)_\alpha$ SSs with different v/v % of SiO_2; Figure S4: IR−ATR spectrum of *h*-Li$(BH_4)_{1-\alpha}(X)_\alpha$ SSs with different v/v % of SiO_2.

Author Contributions: Conceptualization, V.G. and P.d.J.; methodology, V.G. and L.d.K.; validation, P.N., P.d.J. and M.B.; formal analysis, V.G. and P.N.; resources, P.d.J. and M.B.; data curation, V.G. and L.d.K.; writing—original draft preparation, V.G.; writing—review and editing, P.N., P.d.J. and M.B.; supervision, P.d.J.; funding acquisition, P.d.J. and M.B. All authors have read and agreed to the published version of the manuscript.

Funding: P.N. and P.d.J. gratefully acknowledge financial support from "The Netherlands Organization for Scientific Research" (NWO-ECHO and NWO-RELEASE). M.B. acknowledges support from Project CH4.0 under the MUR program "Dipartimenti di Eccellenza 2023–2027" (CUP: D13C22003520001).

Data Availability Statement: The authors declare that data supporting the findings of this study are available within the paper and its Supplementary Information files. Should any raw data files be needed in another format, they are available from the corresponding authors upon reasonable request.

Conflicts of Interest: The authors declare no conflict of interest.

References

1. Goodenough, J.B.; Kim, Y. Challenges for Rechargeable Li Batteries. *Chem. Mater.* **2010**, *22*, 587–603. [CrossRef]
2. Bachman, J.C.; Muy, S.; Grimaud, A.; Chang, H.-H.; Pour, N.; Lux, S.F.; Paschos, O.; Maglia, F.; Lupart, S.; Lamp, P.; et al. Inorganic Solid-State Electrolytes for Lithium Batteries: Mechanisms and Properties Governing Ion Conduction. *Chem. Rev.* **2016**, *116*, 140–162. [CrossRef] [PubMed]
3. Manthiram, A.; Yu, X.; Wang, S. Lithium Battery Chemistries Enabled by Solid-State Electrolytes. *Nat. Rev. Mater.* **2017**, *2*, 16103. [CrossRef]
4. Goodenough, J.B.; Singh, P. Review—Solid Electrolytes in Rechargeable Electrochemical Cells. *J. Electrochem. Soc.* **2015**, *162*, A2387–A2392. [CrossRef]
5. Culver, S.P.; Koerver, R.; Krauskopf, T.; Zeier, W.G. Designing Ionic Conductors: The Interplay between Structural Phenomena and Interfaces in Thiophosphate-Based Solid-State Batteries. *Chem. Mater.* **2018**, *30*, 4179–4192. [CrossRef]
6. Muldoon, J.; Bucur, C.B.; Gregory, T. Quest for Nonaqueous Multivalent Secondary Batteries: Magnesium and Beyond. *Chem. Rev.* **2014**, *114*, 11683–11720. [CrossRef] [PubMed]

7. Ikeshoji, T.; Tsuchida, E.; Morishita, T.; Ikeda, K.; Matsuo, M.; Kawazoe, Y.; Orimo, S.-I. Fast-ionic conductivity of Li+ in LiBH4. *Phys. Rev. B-Condens. Matter Mater. Phys.* **2011**, *83*, 144301. [CrossRef]
8. El Kharbachi, A.; Pinatel, E.; Nuta, I.; Baricco, M. A Thermodynamic Assessment of LiBH4. *Calphad* **2012**, *39*, 80–90. [CrossRef]
9. Matsuo, M.; Nakamori, Y.; Orimo, S.; Maekawa, H.; Takamura, H. Lithium Superionic Conduction in Lithium Borohydride Accompanied by Structural Transition. *Appl. Phys. Lett.* **2007**, *91*, 224103. [CrossRef]
10. Gulino, V.; Wolczyk, A.; Golov, A.A.; Eremin, R.A.; Palumbo, M.; Nervi, C.; Blatov, V.A.; Proserpio, D.M.; Baricco, M. Combined DFT and Geometrical–Topological Analysis of Li-Ion Conductivity in Complex Hydrides. *Inorg. Chem. Front.* **2020**, *7*, 3115–3125. [CrossRef]
11. Gulino, V.; Brighi, M.; Dematteis, E.M.; Murgia, F.; Nervi, C.; Černý, R.; Baricco, M. Phase Stability and Fast Ion Conductivity in the Hexagonal LiBH4–LiBr–LiCl Solid Solution. *Chem. Mater.* **2019**, *31*, 5133–5144. [CrossRef]
12. Asakura, R.; Duchêne, L.; Kühnel, R.-S.; Remhof, A.; Hagemann, H.; Battaglia, C. Electrochemical Oxidative Stability of Hydroborate-Based Solid-State Electrolytes. *ACS Appl. Energy Mater.* **2019**, *2*, 6924–6930. [CrossRef]
13. Sveinbjörnsson, D.; Myrdal, J.S.G.; Blanchard, D.; Bentzen, J.J.; Hirata, T.; Mogensen, M.B.; Norby, P.; Orimo, S.; Vegge, T. Effect of Heat Treatment on the Lithium Ion Conduction of the LiBH4–LiI Solid Solution. *J. Phys. Chem. C* **2013**, *117*, 3249–3257. [CrossRef]
14. Unemoto, A.; Chen, C.; Wang, Z.; Matsuo, M.; Ikeshoji, T.; Orimo, S.I. Pseudo-Binary Electrolyte, $LiBH_4$-LiCl, for Bulk-Type All-Solid-State Lithium-Sulfur Battery. *Nanotechnology* **2015**, *26*, 254001. [CrossRef] [PubMed]
15. Maekawa, H.; Matsuo, M.; Takamura, H.; Ando, M.; Noda, Y.; Karahashi, T.; Orimo, S.-I. Halide-stabilized $LiBH_4$, a room-temperature lithium fast-ion conductor. *J. Am. Chem. Soc.* **2009**, *131*, 894–895. [CrossRef] [PubMed]
16. Matsuo, M.; Remhof, A.; Martelli, P.; Caputo, R.; Ernst, M.; Miura, Y.; Sato, T.; Oguchi, H.; Maekawa, H.; Takamura, H.; et al. Complex Hydrides with $(BH_4)^-$ and $(NH_2)^-$ Anions as New Lithium Fast-Ion Conductors. *J. Am. Chem. Soc.* **2009**, *131*, 16389–16391. [CrossRef] [PubMed]
17. Wang, H.; Bolarin, J.A.; Zhang, B.; Liu, W. Evaluation of a new lithium complex hydride: A derivative of BH4- and NH2- for fast Li-ion conduction and H2 sorption. *Dalton Trans.* **2023**, *accepted manuscript*. [CrossRef] [PubMed]
18. Luo, X.; Rawal, A.; Aguey-Zinsou, K.-F. Investigating the factors affecting the ionic conduction in nanoconfined NaBH4. *Inorganics* **2021**, *9*, 2. [CrossRef]
19. Lefevr, J.; Cervini, L.; Griffin, J.M.; Blanchard, D. Lithium Conductivity and Ions Dynamics in $LiBH_4/SiO_2$ Solid Electrolytes Studied by Solid-State NMR and Quasi-Elastic Neutron Scattering and Applied in Lithium-Sulfur Batteries. *J. Phys. Chem. C* **2018**, *122*, 15264–15275. [CrossRef]
20. Yang, G.; Xie, C.; Li, Y.; Li, H.-W.; Liu, D.; Chen, J.; Zhang, Q. Enhancement of the ionic conductivity of lithium borohydride by silica supports. *Dalton Trans.* **2021**, *50*, 15352–15358. [CrossRef]
21. Gulino, V.; Barberis, L.; Ngene, P.; Baricco, M.; de Jongh, P.E. Enhancing Li-Ion Conductivity in LiBH4-Based Solid Electrolytes by Adding Various Nanosized Oxides. *ACS Appl. Energy Mater.* **2020**, *3*, 4941–4948. [CrossRef]
22. Suwarno, S.; Nale, A.; Suwarta, P.; Wijayanti, I.D.; Ismail, M. Designing Nanoconfined LiBH4 for Solid-State Electrolytes. *Front. Chem.* **2022**, *10*, 866959. [CrossRef]
23. Luo, X.; Rawal, A.; Salman, M.S.; Aguey-Zinsou, K.-F. Core–Shell NaBH4@Na2B12H12 Nanoparticles as Fast Ionic Conductors for Sodium-Ion Batteries. *ACS Appl. Nano Mater.* **2022**, *5*, 373–379. [CrossRef]
24. Choi, Y.S.; Lee, Y.-S.; Oh, K.H.; Cho, Y.W. Interface-enhanced Li ion conduction in a $LiBH_4$-SiO_2 solid electrolyte. *Phys. Chem. Chem. Phys.* **2016**, *18*, 22540–22547. [CrossRef]
25. de Kort, L.M.; Gulino, V.; de Jongh, P.E.; Ngene, P. Ionic Conductivity in Complex Metal Hydride-Based Nanocomposite Materials: The Impact of Nanostructuring and Nanocomposite Formation. *J Alloys Compd.* **2022**, *901*, 163474. [CrossRef]
26. de Kort, L.; Ngene, P.; Baricco, M.; de Jongh, P.; Gulino, V. Improving the Cycle Life of Solid-State Batteries by Addition of Oxide Nanoparticles to a Complex Hydride Solid Electrolyte. *J. Phys. Chem. C* **2023**, *127*, 3988–3995. [CrossRef]
27. Dimitrov, V.; Sakka, S. Electronic Oxide Polarizability and Optical Basicity of Simple Oxides. *J. Appl. Phys.* **1996**, *79*, 1736–1740. [CrossRef]
28. Brunauer, S.; Emmett, P.H.; Teller, E. Adsorption of Gases in Multimolecular Layers. *J. Am. Chem. Soc.* **1938**, *60*, 309–319. [CrossRef]
29. Lutterotti, L.; Matthies, S.; Wenk, H.R. MAUD: A Friendly Java Program for Material Analysis Using Diffraction. *Newsletter CPD* **1999**, *21*, 14–15.
30. Boukamp, B.A. Electrochemical Impedance Spectroscopy in Solid State Ionics: Recent Advances. *Solid State Ion.* **2004**, *169*, 65–73. [CrossRef]
31. Boukamp, B.A. A Package for Impedance/Admittance Data Analysis. *Solid State Ion.* **1986**, *19*, 136–140. [CrossRef]
32. Liu, Z.; Xiang, M.; Zhang, Y.; Shao, H.; Zhu, Y.; Guo, X.; Li, L.; Wang, H.; Liu, W. Lithium Migration Pathways at the Composite Interface of $LiBH_4$ and Two-Dimensional MoS_2 Enabling Superior Ionic Conductivity at Room Temperature. *Phys. Chem. Chem. Phys.* **2020**, *22*, 4096–4105. [CrossRef] [PubMed]
33. Cascallana-Matias, I.; Keen, D.A.; Cussen, E.J.; Gregory, D.H. Phase Behavior in the $LiBH_4$–LiBr System and Structure of the Anion-Stabilized Fast Ionic, High Temperature Phase. *Chem. Mater.* **2015**, *27*, 7780–7787. [CrossRef]
34. Filinchuk, Y.; Chernyshov, D.; Cerny, R. Lightest Borohydride Probed by Synchrotron X-Ray Diffraction: Experiment Calls for a New Theoretical Revision. *J. Phys. Chem. C* **2008**, *112*, 10579–10584. [CrossRef]

35. Paskevicius, M.; Jepsen, L.H.; Schouwink, P.; Černý, R.; Ravnsbæk, D.B.; Filinchuk, Y.; Dornheim, M.; Besenbacher, F.; Jensen, T.R. Metal Borohydrides and Derivatives–Synthesis, Structure and Properties. *Chem. Soc. Rev.* **2017**, *46*, 1565–1634. [CrossRef] [PubMed]
36. Oguchi, H.; Matsuo, M.; Hummelshøj, J.S.; Vegge, T.; Nørskov, J.K.; Sato, T.; Miura, Y.; Takamura, H.; Maekawa, H.; Orimo, S. Experimental and Computational Studies on Structural Transitions in the $LiBH_4$–LiI Pseudobinary System. *Appl. Phys. Lett.* **2009**, *94*, 141912. [CrossRef]
37. Sveinbjörnsson, D.; Christiansen, A.S.; Viskinde, R.; Norby, P.; Vegge, T. The $LiBH_4$-LiI solid solution as an electrolyte in an all-solid-state battery. *J. Electrochem. Soc.* **2014**, *161*, A1432. [CrossRef]
38. Miyazaki, R.; Karahashi, T.; Kumatani, N.; Noda, Y.; Ando, M.; Takamura, H.; Matsuo, M.; Orimo, S.; Maekawa, H. Room Temperature Lithium Fast-Ion Conduction and Phase Relationship of LiI Stabilized $LiBH_4$. *Solid State Ion.* **2011**, *192*, 143–147. [CrossRef]
39. Rude, L.H.; Zavorotynska, O.; Arnbjerg, L.M.; Ravnsbæk, D.B.; Malmkjær, R.A.; Grove, H.; Hauback, B.C.; Baricco, M.; Filinchuk, Y.; Besenbacher, F.; et al. Bromide Substitution in Lithium Borohydride, $LiBH_4$–LiBr. *Int. J. Hydrogen Energy* **2011**, *36*, 15664–15672. [CrossRef]
40. Martelli, P.; Remhof, A.; Borgschulte, A.; Ackermann, R.; Strässle, T.; Embs, J.P.; Ernst, M.; Matsuo, M.; Orimo, S.-I.; Züttel, A. Rotational Motion in $LiBH_4$/LiI Solid Solutions. *J. Phys. Chem. A* **2011**, *115*, 5329–5334. [CrossRef]
41. Buchter, F.; Łodziana, Z.; Mauron, P.; Remhof, A.; Friedrichs, O.; Borgschulte, A.; Züttel, A.; Sheptyakov, D.; Strässle, T.; Ramirez-Cuesta, A.J. Dynamical Properties and Temperature Induced Molecular Disordering of $LiBH_4$ and $LiBD_4$. *Phys. Rev. B* **2008**, *78*, 094302. [CrossRef]
42. Lin, D.; Liu, W.; Liu, Y.; Lee, H.R.; Hsu, P.-C.; Liu, K.; Cui, Y. High Ionic Conductivity of Composite Solid Polymer Electrolyte via In Situ Synthesis of Monodispersed SiO_2 Nanospheres in Poly(Ethylene Oxide). *Nano Lett.* **2016**, *16*, 459–465. [CrossRef] [PubMed]
43. Blanchard, D.; Nale, A.; Sveinbjörnsson, D.; Eggenhuisen, T.M.; Verkuijlen, M.H.W.; Suwarno; Vegge, T.; Kentgens, A.P.M.; De Jongh, P.E. Nanoconfined $LiBH_4$ as a Fast Lithium Ion Conductor. *Adv. Funct. Mater.* **2015**, *25*, 184–192. [CrossRef]